



Wireless image transfer by various antennas using transmitter and receiver modules at 5.8 GHz

Gobind Rai¹, Puneet Sehgal^{1,2} and Kamlesh Patel¹ 

¹Department of Electronic Science, University of Delhi, New Delhi, India and ²Atma Ram Sanatan Dharma College, University of Delhi, New Delhi, India

Research Paper

Cite this article: Rai G, Sehgal P, Patel K (2024) Wireless image transfer by various antennas using transmitter and receiver modules at 5.8 GHz. *International Journal of Microwave and Wireless Technologies*, 1–12. <https://doi.org/10.1017/S1759078724000618>

Received: 14 January 2024

Revised: 20 May 2024

Accepted: 21 May 2024

Keywords:

Blind/Referenceless Image Spatial Quality Evaluator (BRISQUE); C-SRR; graphical user interface; H-SRR; image quality score; metamaterial antenna; orthogonal frequency division multiple access; real-time image transfer; transmitter/receiver module; wireless sensor network

Corresponding author: Kamlesh Patel;
Email: kpatel@south.du.ac.in

Abstract

This research proposes an inexpensive technique for wireless image transfer for security and surveillance applications. The technique uses a 5.8 GHz transmitter and receiver module, along with external antennas in the real-time image transfer within a radius of 100 m. The transferred images are stored in a laptop using a Python code-based graphical user interface application. Different antennas, dipole, circular split-ring resonators, hexagonal split-ring resonators, and metamaterial antennas are utilized for comparison. The Blind/Referenceless Image Spatial Quality Evaluator method is used to assess the picture quality of transferred images to quantify image transfer performance when no ground truth or reference photos are supplied. According to the presented results, images transferred using metamaterial antennas have higher quality than those transferred with other types of antennas. For security considerations, such a system can communicate and store the images in real time.

Introduction

Whenever visual data – such as pictures or videos – is transferred wirelessly between devices, no physical wires are involved. With the use of wireless communication protocols, this technology makes it feasible to send images from a source device – like a camera or sensor – to a destination – like a computer, display, or storage device. Wireless sensor networks (WSNs) have recently become one of the most attractive networking technologies since they have developed without costly communication infrastructures [1]. Such networks are characterized primarily by nodes with limited resources. These nodes comprise communication, data processing, and sensing components. Therefore, sensor nodes are embedded systems that detect their surroundings, gather sensed data, and use multi-hop communication to send it autonomously. However, they are energized by small and irreplaceable batteries and so the sensor nodes have a limited number of bits to be sent during their lifespan due to this energy constraint. Thus, data transmission and consumption of energy are always considered simultaneously in WSNs. When the nodes in a WSN are equipped with cameras, they can be utilized for image-based applications such as data monitoring, streaming video, still images, and surveillance [2, 3]. Because heterogeneous sensor nodes run on batteries, WSNs impose stringent restrictions on the transport of multimedia: restricted memory, low bandwidth, and restricted processing power [4]. The deployment of vision-based sensor networks has been hindered by the lack of appropriate image sensors with integrated data compression capabilities for WSN applications. In reality, WSN nodes find low power consumption to be a far more desirable attribute than the color processing, high resolution, and high frame rates that commercial imagers offer [5]. The possible solutions are low-power microsensor devices with embedded processing capabilities, and an ideal algorithm able to handle data quickly and effectively, with a minimal memory footprint, inexpensive, and provide high-quality compression. Certain conventional image compression techniques, such as JPEG and JPEG2000, are ineffective for wireless multimedia sensor networks (WMSNs) [6, 7] since they do not meet the majority of these requirements.

Initially, a transfer of digital pictures from a standard digital camera or compact flash memory card to a remote Internet site is proposed as a data service using existing Gaussian scale mixture (GSM) networks and mobile phones for the end user [8]. The WMSN is different from the classical wired networks and WSNs in terms of the nature and size of data being transmitted, memory resources, and power consumed per node for processing and transmission. These problems can be overcome by image compression and various recent algorithms of image compression are summarized for the benefits and shortcomings in paper [9]. As the image and video signals take a longer time to transmit, the compression techniques are useful to make the acquired image compatible with the channel bandwidth by reducing the channel noise [10]. For efficient transmission of encrypted images, a comparison between four encryption algorithms is made with different orthogonal frequency division multiplexing (OFDM)

versions like the fast Fourier transform OFDM, the discrete cosine transform (DCT) OFDM, and the discrete wavelet transform (DWT) OFDM [11], which confirms that the performance of all OFDM systems with zero padding schemes is better than that with the cyclic prefix scheme.

A sparse non-orthogonal wavelet division multiplexing (SN-OWDM) scheme is proposed for an underwater acoustic channel, wherein the results confirm that the proposed SN-OWDM scheme needs less frequency resource compared with OFDM with higher peak signal-to-noise ratio and lower peak-to-average power ratio as well [12]. A new joint source and channel coding technique is proposed for wireless image transmission, which directly maps the image pixel values to the complex-valued channel input symbols [13]. Efficient transmission of an encrypted image is achieved through a multiple-input multiple-output (MIMO) OFDM system over an additive white Gaussian noise channel (AWGN) with three different encryption schemes, advanced encryption standard, data encryption standard, and Rubik's cube encryption algorithms [14]. One more application of image communication is a robust color image steganography over wireless communication systems, in which the DCT and DWT is used to increase the sensitivity of extraction of hidden images to the channel degradation effects in an OFDM wireless communication system [15]. To accurately identify the target signal and improve the reliability of wireless image transmission, a wireless image transmission interference signal recognition system is discussed based on deep learning (DL) [16]. Here, STM32F107VT and SI4463 are used as a wireless controller, and the feature vector of the interference signal is evaluated as a time-domain characteristic. Three new transmission schemes of encrypted images are proposed for downlink discrete sine transform-based multi-carrier code division multiple access (DST-MC-CDMA) systems to resolve issues of multipath fading, inter symbol interference, and jitter, especially for such applications [17]. Image reconstruction is reported using B210 Universal Software Radio Peripheral (USRPs) hardware, where an image is transmitted through phase-shift keying (PSK) modulation technique, and found satisfactory by comparing with the transmission of the original image over AWGN channel in the LabVIEW platform [18].

The images transmitted over OFDM suffered from two types of noise, Rayleigh and impulse. A performance evaluation of the transmitted images using statistical (structural similarity image measure, 2D correlation) and information-theoretic (joint histogram measure) properties confirmed that the joint histogram measure has better similarity performance in different modulation schemes utilized such as binary phase-shift keying (BPSK), quadrature phase-shift keying (QPSK), 8-phase-shift keying (PSK) and 16-quadrature amplitude modulation (QAM) [19]. In most image transfer methods or techniques, lower bands of frequency for Wireless Local Area Network (WLAN) and Worldwide Interoperability for Microwave Access (WiMAX) applications are used like 915 MHz, 2.4 GHz, and 3.5 GHz. These communication technologies have limitations of capacity, so the image transfer methods are extensively explored at the higher bands of WLAN and 5G/6G networks. Semantic-oriented communication is one of the most promising methods to enhance bandwidth by only transmitting the semantics of the data, instead of the bit-by-bit reconstruction of the data at the receiver's end. This overcomes the limited bandwidth problems in modern high-volume multimedia transmission like for future 6G communication networks with integration of artificial intelligence. A multilevel semantic aware communication (MLSC) system is proposed based on DL

techniques and trained in an end-to-end manner for wireless image transmission, named MLSC-image [20]. In the study [21], a semantic communication-based end-to-end image transmission system is developed in conjunction with physical channel characteristics, wherein a pre-trained generative adversarial network is used at the receiver to reconstruct the realistic image based on the semantic segmented image. For communication with many Internet of things devices, a federated learning-based semantic communication framework is proposed for multitask distributed image transmission [22]. For wireless secure transmission of images, the ability of different orthogonal frequency division multiple access (OFDMA) systems is extensively investigated on different signal processing techniques, such as DSTs and DCTs, as well as the conventional discrete Fourier transforms (DFTs) with/without Rivest-Shamir-Adleman encryption [23], wherein the results confirm the superiority of DCT-OFDMA system over the DST-OFDMA and the conventional DFT-OFDMA systems.

In the current era, transferring an image with the utmost quality has become an important concern due to its versatile uses. For example, in surveillance and security, object detection and tracking, applying deep/machine learning, and providing high video/image quality to consumers, as well as in forensic and medical applications. A closed-circuit television (CCTV) camera is used at the commercial level for transferring images/video and is extensively employed for surveillance and security applications [24]. In forensic applications, there is often a requirement to extract crucial details from low-resolution CCTV videos and to obtain high-resolution images [25]. Subjective and objective methods are the two primary types of image quality evaluation techniques [26, 27]. Subjective approaches rely on human judgment [28]. Conversely, objective approaches entail explicit numerical criteria comparisons [29, 30]. So, an alternate wireless system for transferring images and video recording is essential for monitoring and security purposes without a visual signature. When the visual signal is transmitted wirelessly rather than through the CCTV, it increases the distortion in the image. These distortions commonly include blur, noise, contrast, and environmental artefacts. After the reception of the image, reliable image quality assessment (IQA) methods are applied preferably with no-reference images as developed for JPG compressed images [31]. Thus, IQA methods are categorized into three types: full-reference IQA [32, 33], reduced-reference IQA [34, 35], and no-reference IQA (NR-IQA) methods [36–38]. The requirement to develop effective NR-IQA methods, which can predict image quality without any reference is on the rise as in most real-time applications, the original reference image is often unavailable. Earlier, a majority of NR-IQA models made use of the natural scene statistics to extract distortion-related features to predict image quality, such as the GSM model in the wavelet domain [39], the Weibull and generalized Gaussian distribution (GGD) model in the DCT domain [40, 41], and a computational framework [42].

New NR-IQA models have been proposed with superior performances, like a novel channel recombination and projection network [43], a two-stage visual interaction perceptual network [44], a no-reference blurred image quality evaluation model mapped into the quality score via support vector regression [45], human visual system based on perceptual features [46]. Many multi-part models like a contrastive distortion-level learning-based NR-IQA framework [47], rotation-invariant and computationally efficient NR-IQA model [48] are reported and compared to test the effectiveness of the proposed NR-IQA model. In the most of reported literature, the performance metrics such as Spearman

rank-ordered correlation coefficient, Pearson linear correlation coefficient, and root mean square error are computed to show the efficiency of the presented model. In some works, the mean opinion score (MOS) and difference MOS are used as the predicted score that matches human perceptions, so the reported method is more accurate, less complex, independent of distortions, and well-suited for real-time applications.

The present work describes an inexpensive wireless image transfer technique for surveillance and security purposes wherein the performance of different antennas is evaluated in real-time scenarios utilizing the 5.8 GHz transmitter and receiver modules. At 5.8 GHz, transmission is based on OFDM technology and IEEE 802.11a protocol, where in transmission rate can reach 54 Mbps/s suitable for high-definition digital images in urban monitoring systems. So, this evaluation-focused technique is valuable for many applications. A Python code based graphical user interface (GUI) is developed to capture and store the received images in the laptop. By employing the Blind/Referenceless Image Spatial Quality Evaluator (BRISQUE) method which is preferably used for comparison in NR-IQA methods, the evaluation offers a standardized approach to assess picture quality without the need for ground truth or reference photos. This methodology is of interest to researchers and practitioners in the field of image processing and wireless communication. The experiment also compares the performance of different antenna types, including dipole antennas, circular split-ring resonators (C-SRRs), hexagonal split-ring resonators (H-SRRs), and metamaterial antennas. Such a comparative analysis provides useful information for practitioners seeking to select the most suitable antenna for their specific application requirements. The analysis's findings indicate that images transferred using metamaterial antennas exhibit higher quality compared to those transferred using other types of antennas.

Proposed image transfer technique

Hardware-transmitter to receiver modules and antennas setup

Figure 1 illustrates a transmitter and receiver module configuration having transmitting and receiving antennas for wireless image capture and transfer.

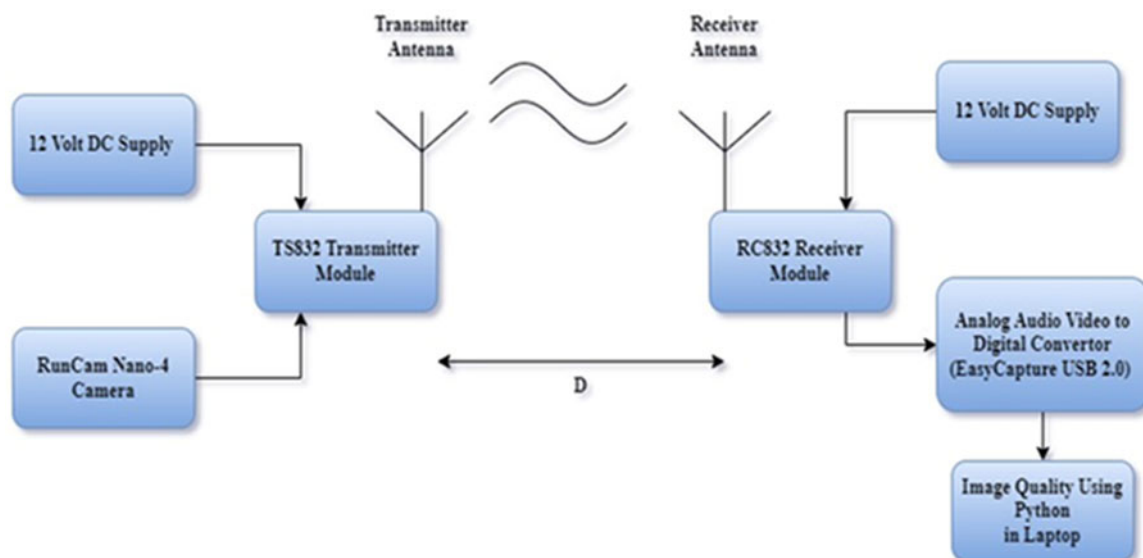


Figure 1. Arrangement of image transferring using TS832 transmitter and RC832 receiver module.

The transmitter and the receiver modules with their respective antennas are placed at a fixed distance D from each other. This handheld transmitter module with battery can move anywhere from the receiver module (with antenna) while varying the distance D up to 5 m with a step size of 0.5 m in different directions. A camera connected to the transmitter module captures real-time images, which are transmitted at a frequency of 5.8 GHz from the transmitter module. The signals are received by the receiver module and processed to give two analog output ports. To de-embed the images in any laptop or desktop computer, an audio/video to USB converter module was used. A stand-alone GUI application is developed to take the picture or image; Figure 2 depicts the operational flow chart. The BRISQUE method is created in Python code to assess the quality of the acquired picture [37]. This BRISQUE method maps the combined data into a numerical value, which is known as the image quality score (IQS) and its value varies from 0 (very good quality) to 100 (very bad quality).

The experiment setup is realized by using transmitter model TS832 audio/video, receiver model RC832 audio/video, a pair of standard dipole antennas, camera model Run Cam Nano 4, and batteries for 12 V DC. These models can transmit/receive the frequency-modulated carrier frequencies in the frequency range (FR)1 band of 5G communication.

Use of BRISQUE method

To evaluate image quality, most of the assessment techniques require a reference image and first, these techniques analyze image structure and identify patterns among its features. However, the BRISQUE method is considered particularly effective as it uses image pixel information to calculate these features [37, 38]. Along with the pairwise product coefficients, the design of the BRISQUE-based model takes into account the NSS of locally normalized brightness coefficients in the spatial domain. The process model, shown in Fig. 3, is developed taking these considerations into account.

The initial step involves subtracting the local mean from the image to obtain locally normalized luminescence, which is then

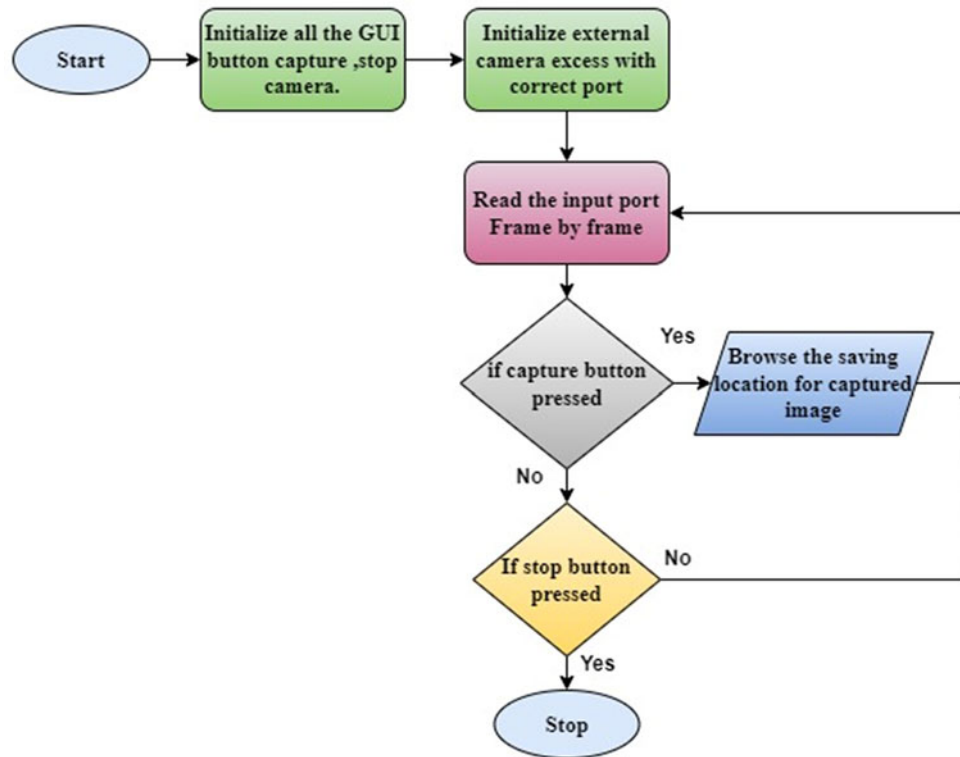


Figure 2. Flowchart of graphical user interface (GUI) for image capturing.

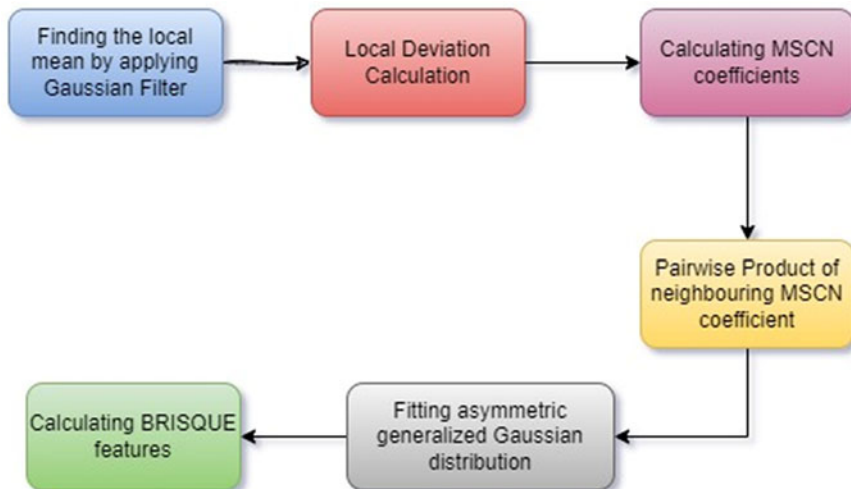


Figure 3. Process model of the BRISQUE method used in this work.

divided by the local deviation. To prevent division by zero, a constant is included. Before computing the mean subtracted contrast normalized (MSCN) coefficients for a grayscale image, it is necessary to first calculate the local mean. The intensity value of the pixel $I(i, j)$ is given by Eq. (1) as

$$\hat{I}(i, j) = \frac{I(i, j) - \mu(i, j)}{\sigma(i, j) + C} \quad (1)$$

where $i \in 1, 2 \dots M, j \in 1, 2 \dots N$ are spatial indices, M and N represent the height and width of the image, respectively. As the denominator gets closer to zero, a constant value of $C = 1$ is used to prevent any instability problems. The terms $\mu(i, j)$ and $\sigma(i, j)$

present the local mean of the pixel's neighborhood and the local standard deviation of the same neighborhood, respectively, and obtained using Eqs. (2) and (3) as follows.

$$\mu(i, j) = \sum_{k=-K}^K \sum_{l=-L}^L w_{k,l} I_{k,l}(i, j) \quad (2)$$

$$\sigma(i, j) = \sqrt{\sum_{k=-K}^K \sum_{l=-L}^L w_{k,l} I_{k,l}(i, j)} \quad (3)$$

where $w = \{w_{k,l}, k = -K, \dots, K, l = -L, \dots, L\}$ is the implementation employs a circularly symmetric 2D Gaussian weighting function, sampled up to 3 standard deviations and

adjusted to have a unit volume. In this case, K and L , which stand for the dimensions of the square window centered on the pixel of interest, are set to 3. The window size is an adjustable parameter that can be set based on the specific use case and the properties of the image.

The pixel's contrast about its immediate neighborhood is represented by the resulting MSCN value, where positive values denote a higher contrast than the mean and negative values represent a lower contrast than the mean. The existence of distortion can affect the distinctive statistical characteristics of MSCN coefficients. By analyzing the changes in the statistical characteristics of an image, one can predict the effect of distortion on the image and its perceived quality. The MSCN coefficients are distributed as a GGD. The density function of the GGD is,

$$f(x; a, \sigma^2) = \frac{a}{2\beta\Gamma\left(\frac{1}{a}\right)} \exp\left(-\left(\frac{|x|}{\beta}\right)^a\right) \quad (4)$$

$$\beta = \sigma \sqrt{\frac{\Gamma(1/a)}{\Gamma(3/a)}} \quad (5)$$

where β is the parameter that affects the shape of the distribution and Γ is the gamma function. The parameter α controls the form and σ^2 is the variance. Pairwise products of neighboring MSCN coefficients along four directions (1) horizontal H , (2) vertical V , (3) main-diagonal $D1$, and (4) secondary-diagonal $D2$ are considered and obtained using Eq. (6)–Eq. (9) as

$$H(i, j) = \hat{I}(i, j) \hat{I}(i, j + 1) \quad (6)$$

$$V(i, j) = \hat{I}(i, j) \hat{I}(i + 1, j) \quad (7)$$

$$D2(i, j) = \hat{I}(i, j) \hat{I}(i + 1, j - 1) \quad (8)$$

$$D2(i, j) = \hat{I}(i, j) \hat{I}(i + 1, j - 1) \quad (9)$$

Since GGD does not fit the empirical histograms of coefficient products well. Therefore, the model is fitted to asymmetric generalized Gaussian distribution. Its density function is given as,

$$f(x; a, \sigma_1^2 \sigma_2^2) = \begin{cases} \frac{v}{(\beta_1 + \beta_2)\Gamma\left(\frac{1}{v}\right)} \exp\left(-\left(\frac{-x}{\beta_1}\right)^v\right), & x < 0 \\ \frac{v}{(\beta_1 + \beta_2)\Gamma\left(\frac{1}{v}\right)} \exp\left(-\left(\frac{x}{\beta_2}\right)^v\right), & x \geq 0 \end{cases} \quad (10)$$

As the BRISQUE approach performs well in real time, is very accurate, and does not require reference images, it is the method preferred for assessing image quality. Equations (1–10) are used to develop a Python code.

Image capturing

Antennas used in the experiments

Four different antennas are employed as seen in Fig. 4, to assess the best antenna preferred for the intended image transfer application. Table 1 lists each antenna's attributes.

C-SRR and H-SRR structures are a Mu-negative type of metamaterial and these structures act like an LC resonance circuit. When such a structure is used in place of a patch in a microstrip antenna [49], it radiates the same resonance frequency with a moderate gain and bandwidth. The resonance or radiated frequency is defined by the physical dimensions of SRRs and the gain between them [50]. A three-layer metamaterial Tx antenna consists of the complementary SRR on the top patch layer, microstrip feed on the middle layer, and grid patterns on the bottom layer and is a type of a double-negative metamaterial which gives wideband and high gain [51], whereas a three-layer metamaterial Rx antenna is made up of three layers: a middle layer of air, a top layer with circular patches etched from the Cu layer as the epsilon near zero layer, and a bottom layer with a rectangular patch of inset-fed microstrip with parasitic elements. It is designed for very high gain with a narrow beam at 5.8 GHz.

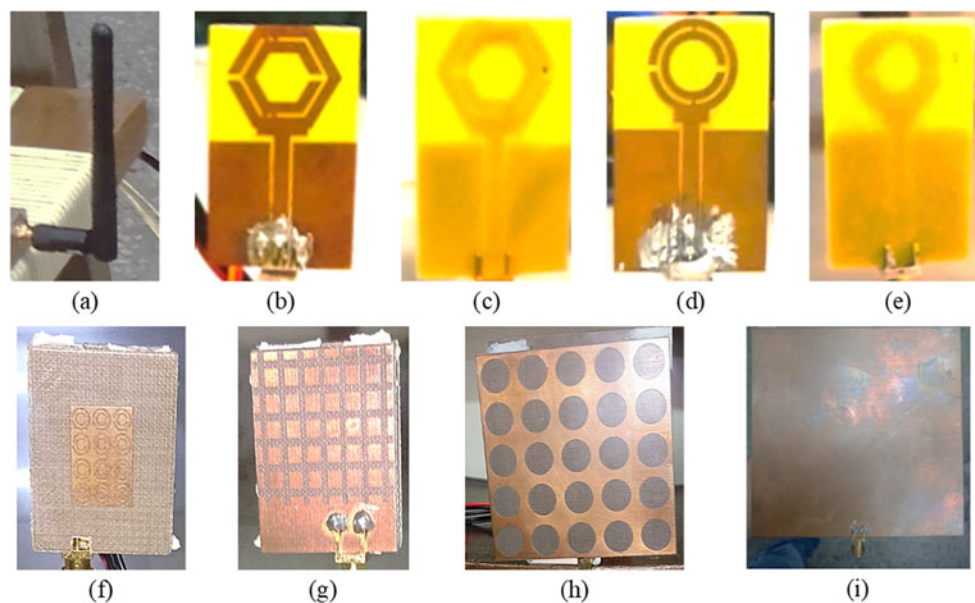


Figure 4. (a) Dipole antenna, (b) front and (c) back side H-SRR antenna, (d) front and (e) backside C-SRR antenna, (f) front and (g) backside metamaterial (double negative index) Tx antenna, (h) front and (i) backside metamaterial (epsilon near zero) Rx antenna.

Table 1. Different antennas and their features

S. No	Used at	Antenna type	Gain (dB)	Frequency (GHz)	Weight (gm)
1.	Transmitter	Dipole	2	5.8	5.934
	Receiver				
2.	Transmitter	Hexagonal split-ring resonator (H-SRR)	2.53	5.8	5.053
	Receiver				
3.	Transmitter	Circular split-ring resonator (C-SRR)	2.51	5.8	5.012
	Receiver				
4.	Transmitter	Metamaterial (double negative index)	5.5	5.8	8.010
	Receiver	Metamaterial (epsilon near zero)	11.4		83.914

Experimental setup for image capturing

Four setups are considered in this study to perform the image transfer as shown in Fig. 4. In these setups, the receiver with antenna is placed in a laboratory on the ground floor of the building, whereas the transmitter with antenna is placed at different locations. In Setup 1, the transmitter is placed horizontally inside the same lab with a varying distance from 0 to 5 m with a step size of 0.5 m (Fig. 5(a)), while in Setup 2 (Fig. 5(b)), the transmitter is placed vertically inside the same lab with a varying 0 to 5 m with step size 0.5 m. In other setups, the transmitter is placed in different locations on the ground floor in the same building (Setup 3) which is represented by flag icons in Fig. 5(c), and the transmitter is placed in different locations on the first floor in the building (Setup 4) represented by flag icons in Fig. 5(d).

First, a pair of dipole antennas are used in all mentioned four setups as shown in Fig. 5(a) and (b), and images are captured, transferred and processed for IQA. In the same manner, a pair of

H-SRR antennas and C-SRR antennas and metamaterial Tx and Rx (MMTR) antennas are used to transfer the images using Setup1 and Setup 3, which are illustrated in Fig. 6.

Image capture GUI app

Python programming has been used to create a GUI, as seen in Fig. 7. This application is capable of capturing images. It is completely a stand-alone application that doesn't require any Python-oriented platform for its functioning. Given the way the developed programming, the user can only select steps to be performed by tapping the buttons on the application. First, double-click on the app icon to start, and a new graphical window will open if the receiver end is already connected to the laptop port, we can see the visuals in the webcam feed sub-window, for capturing the image by pressing the capture button and specify the path by browsing option and we can check the image saved or not using image preview sub window by browsing image.

Results and analysis

As stated earlier, all four antennas are used in the experiments to capture a huge number of photos at various distances and locations. To keep the text concise, some of these photos have been chosen to be shown here. To give a thorough grasp of the picture capture performance, each of these selected photographs is assessed in conjunction with the associated IQS for the particular antenna that was used.

Images transferred using a pair of dipole antennas

The image taken in Setup 2 at a distance of 1 m is shown in Fig. 8, and it has the lowest IQS score of 37.97 out of the four images and is of the highest quality. However, Setups 3 and 4's IQSs of 41.68 and 40.90 demonstrate that the proposed wireless image transfer scheme works regardless of obstructions and orientations.

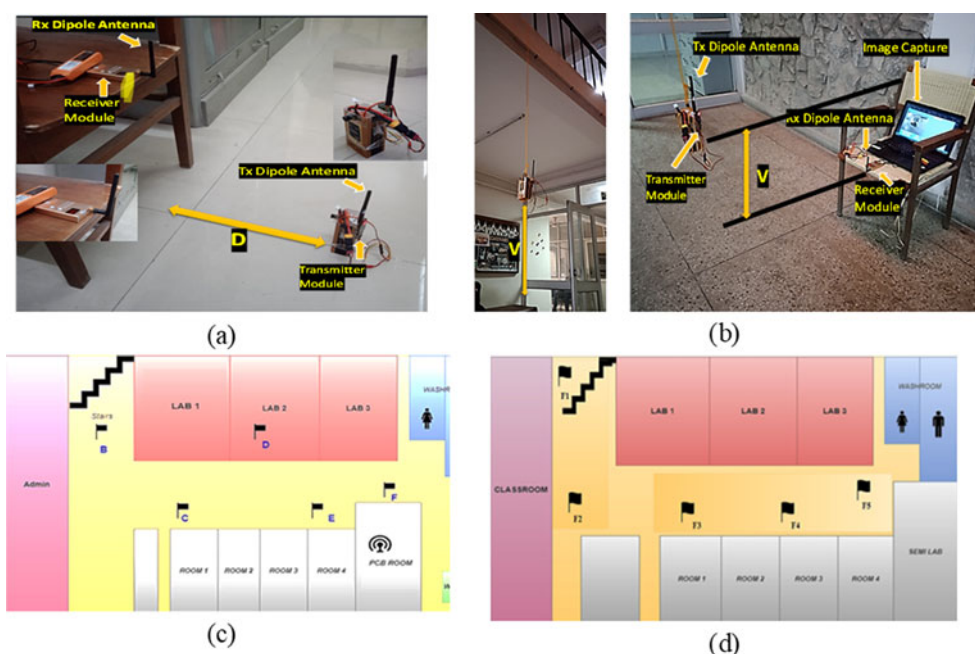


Figure 5. Image transfer using dipole antennas placed in (a) horizontal setup (Setup1), (b) vertical setup (Setup2), (c) ground floor (Setup3), and (d) first floor (Setup4).

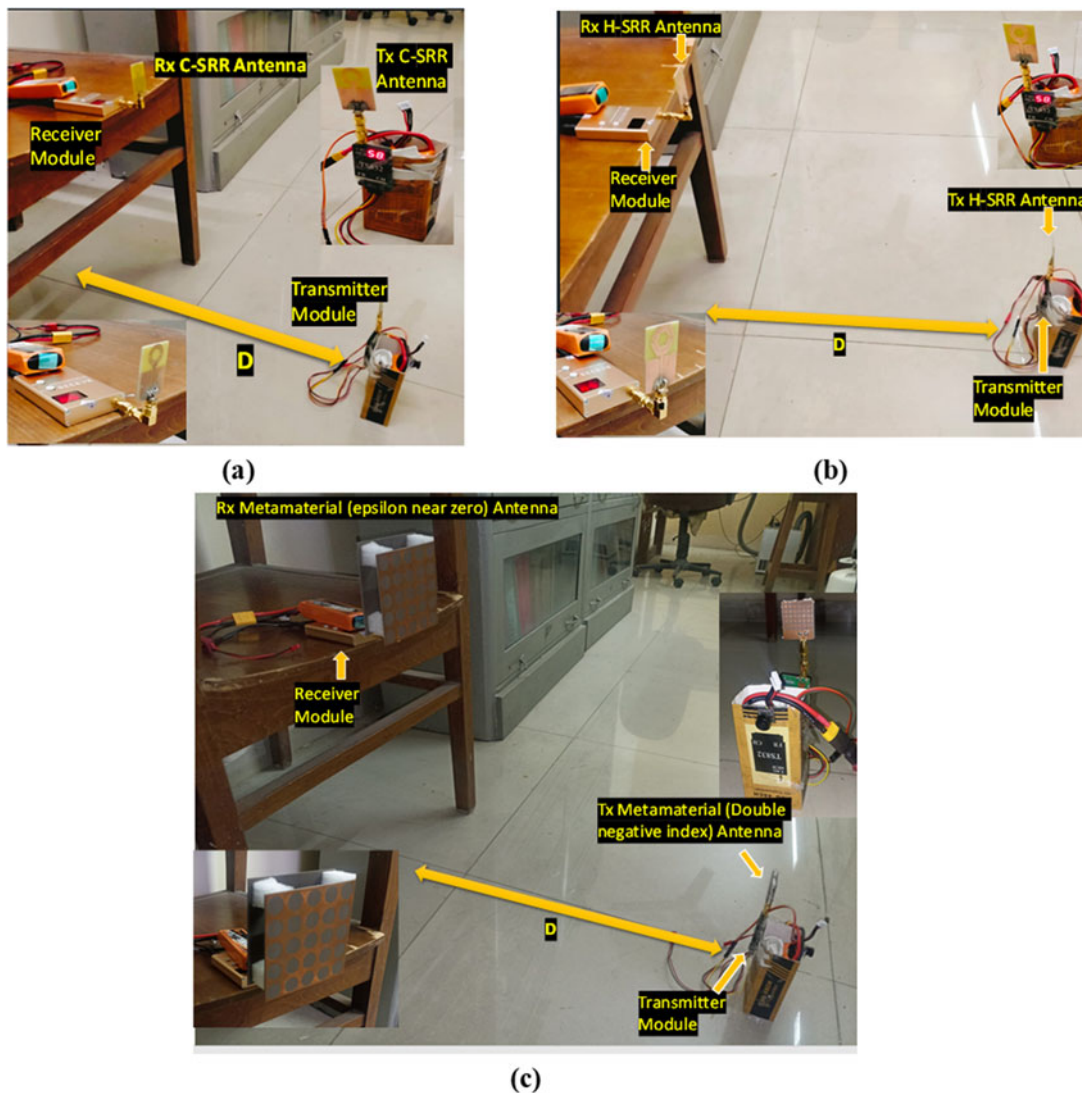


Figure 6. Setup 1 using (a) H-SRR antennas, (b) C-SRR antennas, and (c) metamaterial Tx and Rx antennas.

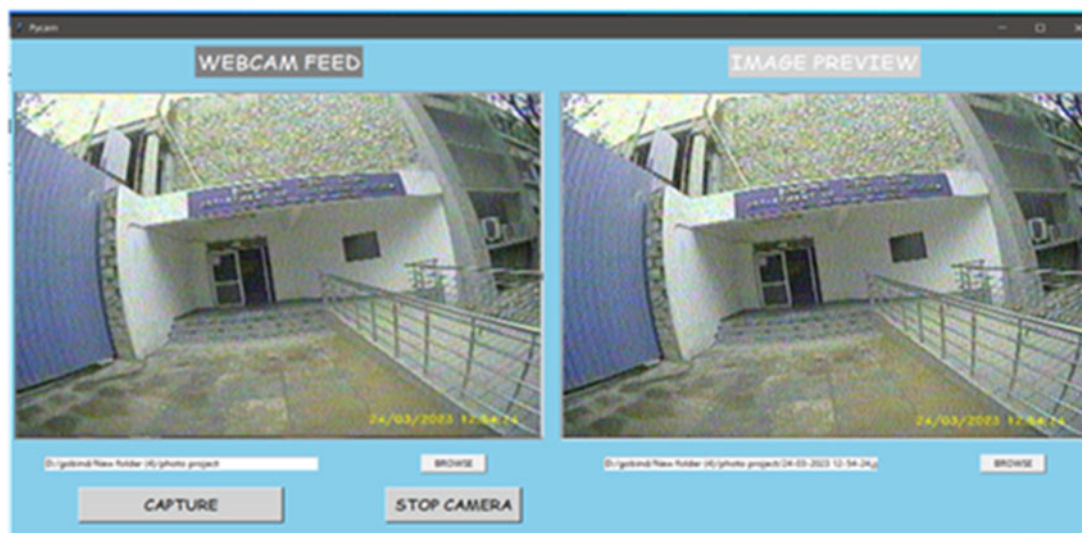


Figure 7. Graphical user interface (GUI) for image capturing.

Setup Image	Setup 1	Setup 2	Setup 3	Setup 4
				
IQS	46.590	37.975595	41.678709	40.902726
Approx. dis/location	1 meter	1 meter	D	F4

Figure 8. IQS of images transferred using a pair of dipole antennas for different setups.













‘D’: 1 meter					
	IQS: 46.590(Dipole)	IQS: 47.329 (H-SRR)	IQS : 48.067(C-SRR)	IQS : 50.49(MMTR)	
	‘D’: 3 meter				
		IQS: 45.196 (Dipole)	IQS: 43.984 (H-SRR)	IQS: 43.346 (C-SRR)	IQS : 42.06(MMTR)
‘D’: 5 meter					
		IQS: 43.658 (Dipole)	IQS: 41.918 (H-SRR)	IQS: 41.990 (C-SRR)	IQS:40.231(MMTR)

Figure 9. Comparison of IQSs of images for Setup 1.

Comparing the effectiveness of different antennas for image transfer

Experiments are carried out using three additional antennas for each of the two setups, Setup 1 and Setup 3, to determine which antenna set is best for the suggested application. For these configurations, the images with their IQS acquired are displayed in Figs. 9 and 10, respectively.

On observing Fig. 9, it is noted that Setup1 with dipole antennas offers the best IQS value of 46.390 than other antennas up to 1 m of distance. For larger distances of 2 and 3 m, the use of MMTR antennas provides IQS values of 42.065 and 40.231, respectively. Figure 10 shows the images and their IQS values obtained in Setup 3. The lowest value of IQS obtained using MMTR antennas confirms that the higher gain antennas with narrow beamwidth (Table 1) are best for wireless image transfer. The higher gain of both three-layer metamaterial antennas with good bandwidth and narrow beam width led to more efficient radiated power transmission and focused reception, which improved the signal transmission/reception than the C-SRR and H-SRR antennas. So, the use of MMTR antennas offered good quality image transfer and a longer range. Additionally, IQS values are thoroughly assessed for every

image utilizing each of the four antenna sets, and the results are shown in Fig. 11. Using Eq. (11) to estimate the variance in IQS values, performances can be evaluated efficiently against the standard dipole.

$$\text{IQS deviation } (\Delta) = \text{IQS of different antennas} - \text{IQS of Dipole Antenna} \quad (11)$$

According to Fig. 11(a), the IQS of the dipole antenna is lower than the IQS of the C-SRR antenna for distances up to 1.5 m and then becomes higher. So, the quality of images obtained using C-SRR antennas is better after these distances. Notably, the IQS of the C-SRR antenna remained relatively constant as the distance between the transmitter and receiver was further increased. Given that Table 1's antenna characteristics are the same for both C-SRR and H-SRR antennas, it can be observed in Fig. 11(b) that the IQS of the H-SRR antenna is comparable to those generated from C-SRR antennas. Again, as in Fig. 11(c), the IQS of the dipole antenna is about 48 and much better than that of the metamaterial (MMTR) antennas for distances up to 1.5 m. After this range, the metamaterial antennas exhibited further lower

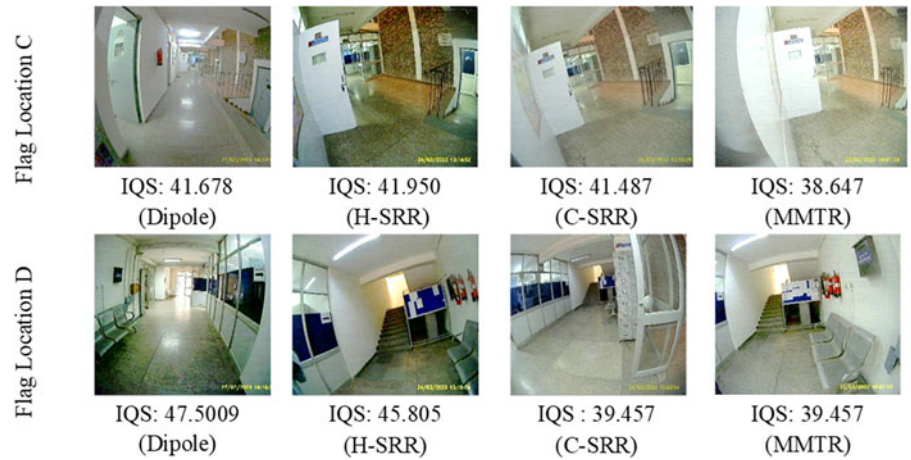


Figure 10. Comparison of IQSs of images for Setup 3.

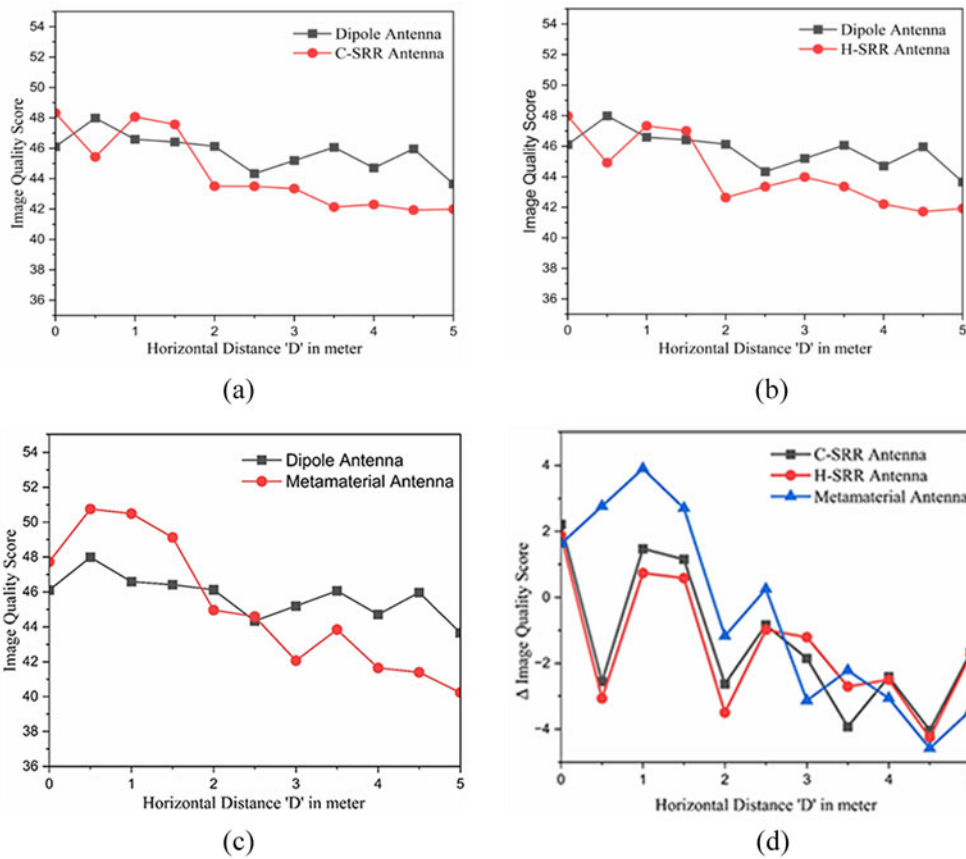


Figure 11. Comparison of image quality score for Setup 1: (a) dipole and C-SRR antennas, (b) dipole and H-SRR antennas, (c) dipole and metamaterial antennas, and (d) IQS deviation with respect to dipole antenna.

values of IQS, which shows that the quality of images gradually enhanced with longer distances while the performance of C-SRR and H-SRR is nearly constant at the same distance. Figure 11(d) shows the IQS deviation (Δ) of different antennas with respect to the dipole antenna. The IQS deviation of the C-SRR and H-SRR antenna is negative for most of the distance, it implies that C-SRR and H-SRR are better than dipole antenna. The IQS deviation of metamaterial antennas is found to be more positive as compared to the other two SRR antennas up to 1.5 m, which implies that the use of metamaterial antennas is unsuitable for very small or close distances. However, after 2 m, the deviation becomes negative

and further negative with distance increases, which confirms the image quality is becoming better using these antennas for longer distances.

To further validate the comparison, images taken at the same locations using four antennas in Setup3 are analyzed and IQS values are shown location-wise of Setup 3 in Fig. 12. Figure 12 confirms that the dipole and C-SRR antennas are providing higher values of IQS in the same floor of building while H-SRR and metamaterial antennas offer better IQS values. In addition, the IQS values obtained using H-SRR and metamaterial antennas remain almost constant and independent of the direction or distance

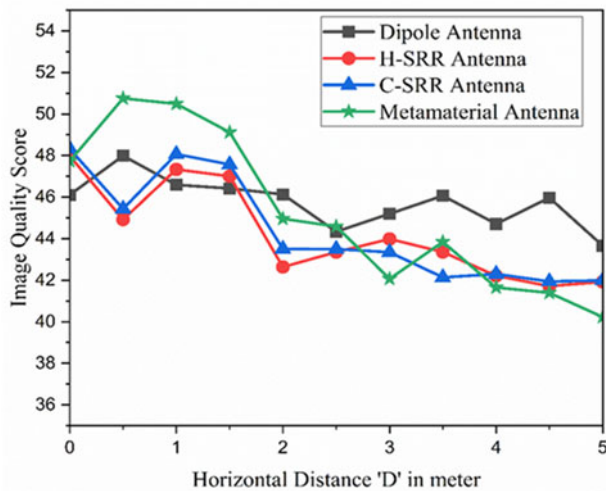


Figure 12. Comparison of IQS for Setup 3.

of the transmitter from the receiver position, even though the metamaterial antennas are more directional. The results show that presented metamaterial antennas are best for the proposed application of wireless image transfer.

To show the novelty in the current research work a comparison with the previously published work is shown in Table 2. In comparison, most of the previous techniques involve complex processing and encryption algorithms to improve the quality of transmitted or encrypted images, whereas the proposed technique of wireless

image transfer is a simple, cheaper, and faster technique that can be implemented with a laptop and a little signal processing. Most of the reported techniques are verified by simulation in various scenarios and modulations, the proposed technique is implemented physically and the quality of received or transferred images is assessed in terms of IQS.

Limitation and future scope

The real-time image quality can be improved further by optimization of antenna designs, including metamaterial antennas, and the use of advanced signal processing methods. These advanced signal processing algorithms are required to enhance image quality by noise reduction, and compression techniques, to minimize data loss during transmission. Also, the optimal deployment and positioning of antennas would maximize signal coverage and minimize signal attenuation, by considering factors such as antenna height, orientation, and spatial arrangement in the surveillance area. Also, in this work, a camera model RunCam Nano 4 is used to keep the proposed application cheaper and handy. By replacing it with a good quality camera, the quality of images can be improved directly. The limitation of the present work is the use of bulky and large-size MMTR antennas for better image quality. In addition to improving the image quality as mentioned in the response to previous comment 7, the new antenna design should focus on the compact high gain and narrow beam width antennas. Also, to increase the range of transmission/reception beyond 100 m, a similar analysis should be performed at a lower frequency like 3.5 GHz in the 5G FR1 band.

Table 2. Comparison of present work with previously published literature

Reference	Op. freq./channel BW	Mod.	Assessment method/parameters	Type of application	System consists of
[18]	915 MHz	QPSK	MSE PSNR	Image transmission	USRP-LabVIEW
[14]	-	BPSK MIMO-OFDM	NPCR UACI	Transmission of encrypted images	Crypto MIMO-OFDM with AWGN channel
[11]	64 MHz BW	QPSK OFDM	PSNR	Image transmission with encrypted algorithms	Carrier frequency offset and compensation
[23]	5 MHz BW	QPSK 16-QAM	MSE PSNR	Transmission of encrypted images	DCT/DST-based OFDMA
[17]	-	CDMA	PSNR MSE	Transmission of encrypted images	DST-based MC-CDMA modulator and demodulator
[21]	-	BPSK	PSNR	Multimedia content transmission	Semantic communication-based end-to-end communication systems
[20]	-	OFDM	PSNR	Image transmission over noisy channel	Multilevel semantic feature extractor
[15]	-	OFDM	PSNR	Image communications	Robust color image steganography
[16]	72 MHz 915 MHz	QAM AM, QPSK, BPSK	Packet loss rate	Signal recognition	NI-USRP 2920, SPM32F107U MCU module, SI403 chip wireless transceiver
This work	5.8 GHz	FM	BRISQUE/IQS	Wireless image transfer	Transmitter TS832 audio/video, receiver RC832 audio/video, a pair of antennas, camera model Run Cam Nano 4.

PSNR = peak signal-to-noise ratio; MSE = mean square error; SSIM = structure similarity index measure; IQS = image quality score; NPCR = number of changing pixel rate; UACI = unified averaged changed intensity.

Conclusion

The present work demonstrated the performance of different antennas in real-time wireless image transfer for surveillance and security purposes using the 5.8 GHz transmitter and receiver commercial modules. The images are taken at different locations and distances from the receiver position. The IQS is obtained using the BRISQUE method and evaluated for all captured images. The results showed that, when it came to wireless image transfer, the metamaterial antenna outperformed any other antenna. Signal quality and intensity are much enhanced in the desired direction due to their directional emission pattern. These findings suggest that to achieve reliable and efficient wireless image transfer for security applications, antenna selection is essential. So, this is the first step for video streaming or video conferencing in real time and in short range without involving other services. In the future, the required modification will be explored to extend the range and quality of images.

Acknowledgements. The work is supported by the Faculty Research Programme (FRP) of the Institute of Eminence (IoE) scheme of the University of Delhi (Letter Ref./No./IoE/2021/12/FRP dated 31.08.2022).

Competing interests. The authors declare that they have no known competing financial interests or personal relationships that could have appeared to influence the work reported in this paper.

References

1. Yang Z, Liao S and Cheng W (2009) Joint power control and rate adaptation in wireless sensor networks. *Ad Hoc Networks* 7(2), 401–410.
2. Yaghmaee MH and Adjeroh DA (2009) Priority-based rate control for service differentiation and congestion control in wireless multimedia sensor networks. *Computer Networks* 53, 1798–1811.
3. Wu H and Abouzeid AA (2005) Energy efficient distributed image compression in resource-constrained multihop wireless networks. *Computer Communications* 28(14), 1658–1668.
4. Zhang W, Deng Z, Wang G, Wittenburg L and Xing Z (2002) Distributed problem-solving in sensor networks. In *Proceedings of the First International Joint Conference on Autonomous Agents and Multiagent Systems*, 988–989.
5. Culurciello E and Andreou AG (2006) CMOS image sensors for sensor networks. *Analog Integrated Circuits and Signal Processing* 49, 39–51.
6. Akyildiz IF, Melodia T and Chowdhury KR (2007) A survey on wireless multimedia sensor networks. *Computer Networks* 51(4), 921–960.
7. Ghorbel O, Jabri I, Ayedi W and Abid M (2011) Experimental study of compressed images transmission through WSN. In *Microelectronics (ICM) 2011 International Conference*, 1–6.
8. Corcoran PM, Bigioi P and Steinberg E (2001) Wireless transfer of images from a digital camera to the internet via a standard GSM mobile phone. *IEEE Transactions on Consumer Electronics* 47(3), 542–547.
9. Eldin HZ, Elhosseini MA and Ali HA (2015) Image compression algorithms in wireless multimedia sensor networks: A survey. *Ain Shams Engineering Journal* 6, 481–490.
10. Chandra M, Agarwal D and Bansae A (2016) Image transmission through wireless channel: A review. In *1st IEEE International Conference on Power Electronics, Intelligent Control and Energy Systems (ICPEICES-2016)*.
11. Eldokany I, El-Rabaie E-SM, Elhalafawy SM, Zein Eldin MA, Shahieen MH, Soliman NF, El-Bendary MA, El-Naby MA, Al-Kamali FS, Elashry IF and Abd El-Samie FE (2015) Efficient transmission of encrypted images with OFDM in the presence of carrier frequency offset. *Wireless personal Communications* 84, 475–521.
12. Zhang J, Ma X, Fu X and Yang J (2019) Sparse nonorthogonal wavelet division multiplexing for underwater sonar image transmission. *IEEE Transactions on Vehicular Technology* 68(12), 11806–11815.
13. Boursoulatz E, Kurka DB and Gündüz D (2019) Deep joint source-channel coding for wireless image transmission. *IEEE Transactions on Cognitive Communications and Networking* 5(3), 567–579.
14. Dharavathu K and Mosa SA (2020) Efficient transmission of an encrypted image through a MIMO-OFDM system with different encryption schemes. *Sensing and Imaging* 21, 13.
15. Eyssa AA, Abdelsamie FE and Abdelnaiem AE (2020) An efficient image steganography approach over wireless communication system. *Wireless Personal Communications* 110, 321–337.
16. Guo Z and Liu S (2021) Wireless image transmission interference signal recognition system based on deep learning. *Wireless Communications and Mobile Computing* 2021, 8024953.
17. Al-Kamali FS, Al-Junaid AF and Al-Shamri MYH (2021) New image transmission schemes for DST-Based MC-CDMA system. *Arabian Journal for Science and Engineering* 46, 1465–1479.
18. Smitha N, Tarun ES, Eswar KS, Reddy NTK and Nagendra P (2022) Image transmission using USRP through LabVIEW. In *2022 IEEE North Karnataka Subsection Flagship International Conference (NKCon)*, Vijaypur, India, 1–6.
19. Dihin RA, Alharan AFH, Abdulameer MH and Ali NS (2022) Evaluation the performance of statistical and information-theoretic properties over FFT-OFDM. In *2022 5th International Conference on Engineering Technology and its Applications (IICETA)*, Al-Najaf, Iraq, 52–57.
20. Zhang Z, Yang Q, He S, Sun M and Chen J (2022) Wireless transmission of images with the assistance of multi-level semantic information. In *2022 International Symposium on Wireless Communication Systems (ISWCS)*, Zhejiang University, Zhejiang, China.
21. Lokumarambage MU, Gowrisetty VSS, Rezaei H, Sivalingam T, Rajatheva N and Fernando A (2023) Wireless end-to-end image transmission system using semantic communications. *IEEE Access* 11, 37149–37163.
22. Xie B, Wu Y, Ng DWK and Zhang W (2023) Communication-efficient framework for distributed image semantic wireless transmission. *IEEE Internet of Things Journal* 10(24), 22555–22568.
23. Abdul F, Al-Fahaidy K, Al-Bouthigy R, Yahya M, Al-Shamri H and Abdulkareem S (2024) Secure image transmission through LTE wireless communications systems. *EURASIP Journal on Image & Video Processing* 2024, 3.
24. Norris C and Armstrong G (1999) *The Maximum Surveillance Society: The Rise of CCTV*. Oxford: Berg.
25. Min H, Lee SH, De Neve W and Ro YM (2013) Improved license plate recognition for low-resolution CCTV forensics by integrating sparse representation-based super-resolution. In *Digital-Forensics and Watermarking. International Workshop on Digital Watermarking*, LNCS8389, 452–462.
26. Kreis R (2004) Issues of spectral quality in clinical H-magnetic resonance spectroscopy and a gallery of artifacts. *NMR in Biomedicine* 17(6), 361–381.
27. Avcibas I, Sankur B and Sayood K (2002) Statistical evaluation of image quality measures. *Journal of Electronic Imaging* 11(2), 206–223.
28. Farrell JE (1999) Image quality evaluation. In MacDonald LW and Luo MR (eds), *Colour Imaging: Vision and Technology*. West Sussex: John Wiley & Sons Inc, 285–313.
29. Cadik M and Slavik P (2004) Evaluation of two principal approaches to objective image quality assessment. In *8th International Conference on Information Visualisation*, IEEE Computer Society Press, 513–551.
30. Nguyen TB and Ziou D (2000) Contextual and non-contextual performance evaluation of edge detectors. *Pattern Recognition Letters* 21(9), 805–816.
31. Wang Z, Sheikh HR and Bovik AC (2002) No-reference perceptual quality assessment of JPEG compressed images. In *Proceedings. International Conference on Image Processing I*.
32. Wang Z, Bovik AC, Sheikh HR and Simoncelli EP (2004) Image quality assessment: From error visibility to structural similarity. *IEEE Transactions on Image Processing* 13(4), 600–612.
33. Kim W, Nguyen A-D, Lee S and Bovik AC (2020) Dynamic receptive field generation for full-reference image quality assessment. *IEEE Transactions on Image Processing* 29, 4219–4231.

34. **Golestaneh S and Karam LJ** (2016) Reduced-reference quality assessment based on the entropy of DWT coefficients of locally weighted gradient magnitudes. *IEEE Transactions on Image Processing* **25**(11), 5293–5303.
35. **Wan Z, Gu K and Zhao D** (2020) Reduced reference stereoscopic image quality assessment using sparse representation and natural scene statistics. *IEEE Transactions on Multimedia* **22**(8), 2024–2037.
36. **Choi MG, Jung JH and Jeon JW** (2009) No-reference image quality assessment using blur and noise. *International Journal of Electronics and Electrical Engineering* **3**, 318–322.
37. **Mittal A and Bovik AC** (2012) No-reference image quality assessment in the spatial domain. *IEEE Transactions on Image Processing* **21**(12), 4695–4708.
38. **Chawdhary A, Kumari S, Bhavsar A and Verma R** (2018) No reference evaluation in super-resolution for CCTV footage. In *IEEE 13th International Conference on Industrial and Information Systems (ICIIS)*.
39. **Moorthy AK and Bovik AC** (2011) Blind image quality assessment: From natural scene statistics to perceptual quality. *IEEE Transactions on Image Processing* **20**(12), 3350–3364.
40. **Yang X, Li F, Zhang W and He L** (2018) Blind image quality assessment of natural scenes based on entropy differences in the DCT domain. *Entropy* **20**(12), 885–906.
41. **Saad MA, Bovik AC and Charrier C** (2012) Blind image quality assessment: A natural scene statistics approach in the DCT domain. *IEEE Transactions on Image Processing* **21**(8), 3339–3352.
42. **Yang X, Li F, Gu K and Liu H** (2022) Study of natural scene categories in measurement of perceived image quality. *IEEE Transactions on Instrumentation and Measurement* **71**, 1–12.
43. **Shen L, Zhao B, Pan Z, Peng B, Kwong S and Lei J** (2022) Channel recombination and projection network for blind image quality measurement. *IEEE Transactions on Instrumentation and Measurement* **71**, 1–12.
44. **Wang X, Xiong J and Lin W** (2023) Visual interaction perceptual network for blind image quality assessment. *IEEE Transactions on Multimedia* **25**, 8958–8971.
45. **Chen J, Li S, Lin L, Wan J and Li Z** (2023) No-reference blurred image quality assessment method based on structure of structure features. *Signal Processing: Image Communication* **118**, 117008.
46. **Rajavelthra J and Gaidhane VH** (2023) A no-reference image quality assessment model based on neighborhood component analysis and Gaussian process. *Journal of Visual Communication and Image Representation* **98**(11), 104041.
47. **Wei X, Li J, Zhou M and Wang X** (2022) Contrastive distortion-level learning-based no-reference image-quality assessment. *International Journal of Intelligent Systems* **37**, 8730–8746.
48. **Rajavelthra J and Gaidhane VH** (2022) An efficient approach for no-reference image quality assessment based on statistical texture and structural features. *Engineering Science and Technology* **30**, 101039.
49. **Sehgal P and Patel K** (2021) Performance analysis and impedance modeling of rectangular and circular split-ring resonator antennas in 2.4/5.2 GHz bands. *Progress in Electromagnetics Research C* **117**, 159–171.
50. **Sehgal P and Patel K** (2023) Dual-band hexagonal SRR antennas and their applications in SIMO and MISO-based WLAN/WiMAX systems. *Progress in Electromagnetics Research B* **99**, 139–157.
51. **Yilmaz HÖ and Yaman F** (2020) Metamaterial antenna designs for a 5.8-GHz Doppler radar. *IEEE Transactions on Instrumentation and Measurement* **69**(4), 1775–1782.



Kamlesh Patel received his M.Sc. degree in Electronics and M.Tech degree in Microwave Electronics from Rani Durgavati Vishwavidyalaya, Jabalpur, India, and the University of Delhi, India, in 1999 and 2003, respectively. He holds Ph.D. from the Delhi Technological University, Delhi, India. From 2004 to 2013, he had worked as scientist with CSIR-National Physical Laboratory, India. Since 2013, he has been working with the

Department of Electronic Science, University of Delhi South Campus, New Delhi, India, where he is now an associate professor. His research interests include microwave components, material characterization, and planar antennas for mobile communications.



Gobind Rai received B.Sc. degree in Electronics Science from Maharaja Agrasen College, which is affiliated with Delhi University (DU), Delhi 110096, India, in 2021, and an M.Sc. degree in Electronics from the Department of Electronic Science, University of Delhi, South Campus, New Delhi, India, in 2023.



Puneet Sehgal received his B.Sc. (Hons.) and M.Sc. degree in Electronics from University of Delhi, India, in 2009 & 2011 respectively. He is currently pursuing Ph.D. degree (Electronics) with Department of Electronic Science, University of Delhi (South Campus), New Delhi. He is currently working as an assistant professor in Department of Electronics, Atma Ram Sanatan Dharma College, University of Delhi.